Experimental investigation on the seismic behavior of RC double-column medium-height bents retrofitted with SCEB-Us

Huihui Dong[1], Xiao Hu[2], Kaiming Bi[3], Qiang Han[4], Alireza Entezami[5], Xiuli Du[5]

1. Associate Professor, State Key Laboratory of Bridge Engineering Safety and Resilience, Beijing University of Technology, Beijing 100124, China. Email: donghh@bjut.edu.cn

2. Doctoral Candidate, State Key Laboratory of Bridge Engineering Safety and Resilience, Beijing University of Technology, Beijing 100124, China. Email: huuxxiao@163.com

3. Associate Professor, Department of Civil and Environmental Engineering, Hong Kong Polytechnic University, Kowloon, Hong Kong 999077, China (corresponding author). Email: kaiming.bi@polyu.edu.hk

4. Professor, State Key Laboratory of Bridge Engineering Safety and Resilience, Beijing University of Technology, Beijing 100124, China. Email: qhan@bjut.edu.cn

5. Assistant professor, Department of Civil and Environmental Engineering, Politecnico di Milano, Milano 20133, Italy. Email: alireza.entezami@polimi.it.

6. Professor, State Key Laboratory of Bridge Engineering Safety and Resilience, Beijing University of Technology, Beijing 100124, China. Email: duxiuli@bjut.edu.cn

Abstract

Two columns of RC double-column medium-height bents (DCMBs) are normally connected by link beams to enhance the lateral stability. Serious damage and/or large residual displacement were repeatedly observed in the DCMBs after major earthquakes, which may make the bridges lose traffic functionality or even be demolished and rebuilt. To enhance the seismic performance of bridge structures with DCMB with link beams, the self-centering energy dissipation braces (SCEBs) were applied to the DCMB in the "K"-shaped arrangement scenario to replace the traditional link beams in this study. To this end, the design philosophies of the SCEBs in the DCMB were first developed based on the configuration and force analysis of the DCMB with SCEBs. Then, 1:4 scaled RC DCMB and DCMB with link beams specimens were designed. Based on the design philosophies and the hysteretic performance of the DCMB, a novel SCEB with U-shaped steel plates (SCEB-U) was developed and tested, and the test results showed that the SCEB-U exhibited a typical flag-shaped hysteretic behavior with great deformation capacity. Subsequently, the quasi-static cyclic loading test of the DCMB with SCEBs specimen was carried out, and a DCMB with link beams and a DCMB with energy dissipation braces with U-shaped steel plates (DCMB with EDB-Us) were also tested for comparison. The experimental results showed that the DCMBs with braces suffered the least damage compared with the DCMB with link beams, and there was no obvious damage in the column-brace connection regions. The DCMB with SCEB-Us exhibited excellent flag-type hysteresis behavior with large carrying capacity, stable energy dissipation, and satisfactory self-centering ability.

KEYWORDS

RC double-column medium-height bent with SCEBs, SCEB-U, damage pattern, hysteretic behavior, residual displacement, quasi-static cyclic loading tests

1 INTRODUCTION

RC bridges with double-column medium-height bents (DCMBs) with link beams have been widely built in mountainous areas to overcome transportation obstacles. As the primary load-bearing member of such bridge structures, RC DCMB with link beams has a simple structural configuration and good structural stability. They are lightweight while saving on the amount of steel and concrete. In addition, the double-column bents are more stable and can accommodate more vehicle lanes by supporting a wider superstructure compared with single-column bents.

In the DCMB with link beams, the link beams distributed vertically at certain height intervals are normally applied to connect the two columns to maintain the adequate lateral stiffness and stability of the bents. In particular, the link beams as ductile members can also improve the seismic performance of the bridge structure in the transverse direction. Under strong earthquakes, the link beams are designed to be damaged before the columns, through their plastic damage, to dissipate some of the seismic energy. Seismic damage investigations[1] showed that the DCMBs with link beams were extremely vulnerable to damage, and the damage areas of such bents were mainly concentrated in the link beam ends and/or the column-beam joints. Once the link beams were severely damaged and destroyed, the transverse connection between the two columns of the bent was lost, resulting in the collapse of the structure. In addition, it is very difficult to repair and maintain the damaged link beams after earthquakes. Notably, seismic damage to the bridges after severe earthquakes may significantly impede post-earthquake rescue and restoration, which imposes substantial threats to the life safety and economic well-being of our society.

Given the severe damage to structures under earthquakes, there is a lot of research on the seismic response of structures under earthquakes, improving seismic resilience, and achieving damage controllability[2-6]. Providing reliable methods for enhancing the seismic performance of bridges with DCMBs with link beams is very critical for life and economic protection. The application of replaceable dampers for the bridge based on the structural fuse concept is considered a reliable method. Structural fuses protect the main structure by dissipating seismic energy before the primary structure yields and enters a plastic state, and damaged structural fuses can be easily replaced. For example, EI-Bahey et al.[7-9] proposed to arrange sacrificial members (buckling-restrained braces, namely BRBs, which are normally used as energy dissipation devices) in a composite concrete-filled steel double-column bent and carried out quasi-static reciprocating loading tests of the bent with BRBs. The test results demonstrated that the BRBs can effectively enhance the stiffness, strength, and energy dissipation capability of the bent. Subsequently, the seismic performance of the bridges retrofitted with energy dissipation dampers was further investigated through numerical simulation[11-16]. Chen et al.[11] assess the seismic performance of tall pier bridges with double-column bents retrofitted with BRBs subjected to near-fault ground motions. Xiang et al.[12] investigated the effect of multi-story brace distribution on the seismic performance of RC tall bridge bents retrofitted with BRBs. These investigations demonstrated that the energy dissipation dampers can not only increase the stiffness and strength of the pier and dissipate earthquake-induced energy, resulting in significantly mitigating seismic responses of the bridges, but they can also be easily and quickly replaced post-earthquake. It should be noted that all the previous studies explored the seismic performance of middle and tall double-column piers or whole bridge structures with additional energy dissipation dampers (EDBs) through numerical simulations, while experimental research has rarely been reported. Furthermore, it is found that the structure with the EDBs may have large residual displacements after a strong earthquake[13]. The large residual displacements significantly affect serviceability and repairability and may even cause the closure of a bridge, which is often accompanied by significant socioeconomic losses induced by traffic flow capacity disruption and repair costs[14-18].

To mitigate the residual drifts and improve the serviceability and repairability of the bridge structure and building structures after earthquakes, some novel self-centering energy dissipation braces (SCEBs) have been widely developed[19-25] and applied[26-45]. Xiang and Alam[39] numerically investigated that SCEBs are effective in reducing the vulnerability of the RC bridge bent at different damage states under either near-fault or far-field ground motions. Upadhyay et al.[40] presented the numerical results that the retrofit strategy with SCEBs can improve the seismic performance of the RC bent. In particular, SCEBs can significantly reduce the residual drift ratio (DR). Dong et al.[41-44] conducted quasi-static tests of RC double-column bents retrofitted using SCEBs and further assessed the seismic performance of bridge structures with SCEBs in both longitudinal and transverse directions, as well as the failure probabilities at different damage states. Recently, Dong et al.[43] numerically investigated the seismic performance of RC bridges with double-column medium-height bents with SCEBs. However, the above research

mainly focused on bridge bents with single-story SCEBs, and to the best of the authors' knowledge, the experimental investigation on the seismic behavior of RC double-column medium-height bents with SCEBs in the form of a double K-brace system has not yet been fully reported in the literature. To study the damage model and hysteretic behaviour of such bents, the quasi-static cyclic loading tests of DCMBs with SCEBs in the form of multiple stories were carried out in this study. This study can provide valuable data to explicitly examine the effect of SCEBs in the form of multiple stories on the seismic performance of DCMBs. It can also serve as a benchmark to validate the numerical models for further, more detailed analyses.

The structure of this article is organized as follows: First, the design philosophies of the SCEBs in the DCMB are developed based on the configuration and force analysis of the DCMB with SCEBs in Sect. 2. Then, the design details of the 1/4 scaled RC DCMB and DCMB with link beams specimens are introduced in Sect. 3. Subsequently, based on the design philosophies and the hysteretic performance of the DCMB, a novel SCEB with U-shaped steel plates (SCEB-U) is developed, and its hysteretic behaviour is tested; meanwhile, an energy dissipation brace with U-shaped steel plates (EDB-U) is also considered for comparison in Sect. 4. In Sect. 5, the SCEB-Us/EDB-Us are applied in the DCMBs instead of the traditional link beams, and the quasi-static cyclic loading tests of the DCMBs with SCEB-Us/EDB-Us are performed to investigate the seismic performance. For comparison, the DCMB with link beams is also tested, and the results are compared in detail with the DCMBs with SCEB-Us/EDB-Us. Finally, some concluding remarks are given in Sect. 6.

2 DESIGN PHILOSOPHIES OF SCEB IN DCMB

To enhance the seismic performance of the bridge with DCMBs, the SCEBs are applied to the DCMBs in a K-shaped form along the height of the column instead of the traditional link beams. The DCMB with SCEBs consists of a cap beam, a foundation, two medium-height columns, and some replaceable SCEBs, as illustrated in Figure 1. The replaceable braces, as the fuse element, should yield before the bent. In the conventional RC double-column bridge piers, damage zones may occur at the beam-column connection locations and the top and bottom of the column. To avoid concentrating the forces at the connecting locations, the braces and the columns are connected by pin connections. The braces are allowed to rotate freely and can be easily replaced after damage. This design limits the moment development at the connection and guarantees that the braces are subject to axial load only. As shown in Figure 1, the gusset plates are fixed to the built-in fittings in cap beams, foundations, and columns, and the anchorage plates of the brace are attached to the gusset plates by steel pins.

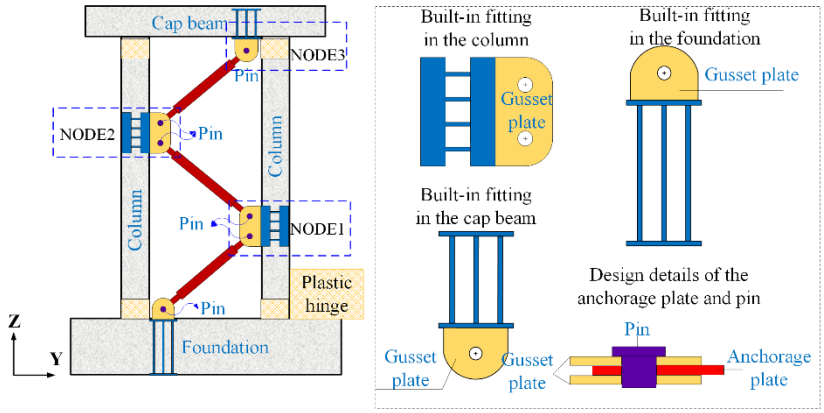

FIGURE 1 Configuration of the DCMB with braces.

2.1 FORCE ANALYSIS

Figure 2A shows the deformation relationship between the three SCEBs and the two columns in the DCMB with SCEBs under the horizontal load from left to right. It is assumed that the linear stiffness of the two columns of the bent is equal, and the lateral deformation of the column increases linearly along the column height before yielding. When the lateral deformation of this bent is X, the axial deformations of the three braces are respectively given by:

$$\Delta S_1 = \sqrt{(L_1 + X_1)^2 + h_1^2} - \sqrt{L_1^2 + h_1^2} \tag{1}$$

$$\Delta S_2 = \sqrt{L_1^2 + h_2^2} - \sqrt{(L_1 + X_1 - X_2)^2 + h_2^2} \tag{2}$$

$$\Delta S_3 = \sqrt{(L_1 + X - X_2)^2 + h_3^2} - \sqrt{L_1^2 + h_3^2} \tag{3}$$

Where ΔS_1, ΔS_2 and ΔS_3 are the axial deformation of SCEB1, SCEB2, and SCEB3, X_1, X_2 and X are the horizontal displacement of NODE1, NODE2, and NODE3, and X_1 and X_2 can be calculated as:

$$\begin{cases} X_1 = h_1 \cdot X / H \\ X_2 = (h_1 + h_2) \cdot X / H \end{cases} \tag{4}$$

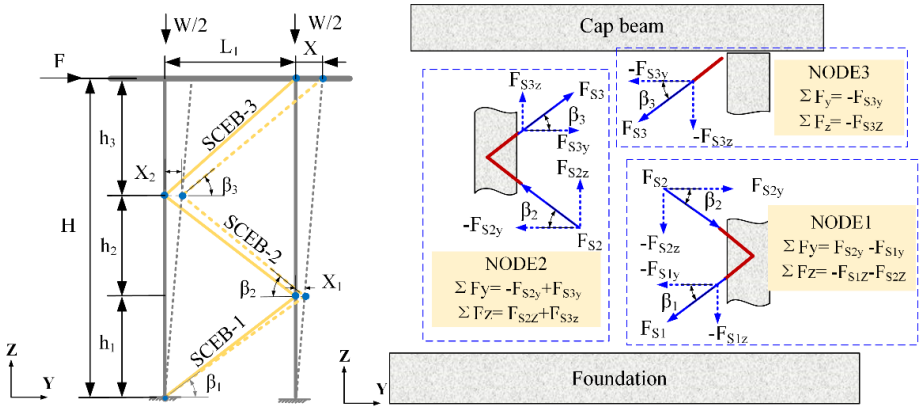

(A) (B)

FIGURE 2 DCMB with SCEBs under the horizontal load (A) deformation pattern; (B) force analysis diagram.

From Figure 2A, it can be seen that SCEB1 and SCEB3 are under tension and SCEB2 is under compression when the DCMB with SCEBs is under the horizontal load from left to right. As shown in Figure 2, the force and stiffness relationships between DCMB with SCEBs, DCMB, and SCEBs in the horizontal direction satisfy the following equations:

$$\begin{aligned} F_{\text{DCMB-SCEB}} &= F_{\text{DCMB}} + F_{\text{SCEB3}} \cdot cos\,\beta_3 + (F_{\text{SCEB2}} \cdot cos\,\beta_2 - F_{\text{SCEB3}} \cdot cos\,\beta_3) + (F_{\text{SCEB1}} \cdot cos\,\beta_1 - F_{\text{SCEB2}} \cdot cos\,\beta_2) \\ &= F_{DCMB} \times X + F_{SCEB1} \times cos\,\beta_1 \end{aligned} \tag{5}$$

in which,

$$F_{\text{DCMB-SCEB}} = K_{\text{DCMB-SCEB}} \cdot X \tag{6}$$

$$F_{\text{DCMB}} = K_{\text{DCMB}} \cdot X \tag{7}$$

$$F_{\text{SCEB1}} = K_{\text{SCEB1}} \cdot \Delta S_1 \tag{8}$$

$$K_{\text{DCMB-SCEB}} \cdot X = K_{\text{DCMB}} \cdot X + K_{\text{SCEB1}} \cdot \Delta S_1 \cdot cos\,\beta_1 \tag{9}$$

where K_{DCMB} is the lateral stiffness of DCMB; K_{SCEB1}, K_{SCEB2} and K_{SCEB3} are the axial stiffness of the three braces, respectively; $K_{\text{DCMB-SCEB}}$ is the lateral stiffness of DCMB with SCEBs; F_{DCMB} is the lateral force of DCMB; F_{SCEB1}, F_{SCEB2} and F_{SCEB3} are the axial force of the three braces; $F_{\text{DCMB-SCEB}}$ is the lateral bearing capacity of DCMB with SCEBs, β_1, β_2 and β_3 are respectively the angle between the three braces and the horizontal direction. From the above analysis, it can be found that when DCMBs are retrofitted with inverted-K SCEBs, only the first layer of the brace provides lateral force for the bent.

It is worth noting that the horizontal force components of the two braces acting on the column can cancel each

other out when the axial forces of the two braces are equal to each other, as can be seen from Figure 2B. This design can protect the column from being damaged.

2.2 DESIGN PHILOSOPHY

Based on the configuration and force analysis of the DCMB with SCEBs, the DCMB with SCEBs can be regarded as the parallel combination of the DCMB and the first layer of the SCEB, since only the first layer of the brace provides effective strength and stiffness for the bent as mentioned before. The hysteretic behavior of the DCMB with SCEB is a superposition of the hysteretic behavior of the DCMB and the first layer of the SCEB, as shown in Figure 3. In Figure 3, Δ_{B-Y} and Δ_{S-Y} are the yield displacements of DCMB and SCEB, respectively; F_{S-C} is the self-centering force of SCEB, respectively; F_{B-P} (at point B) is the restoring force of the DCMB when the displacement of the bent top is zero.

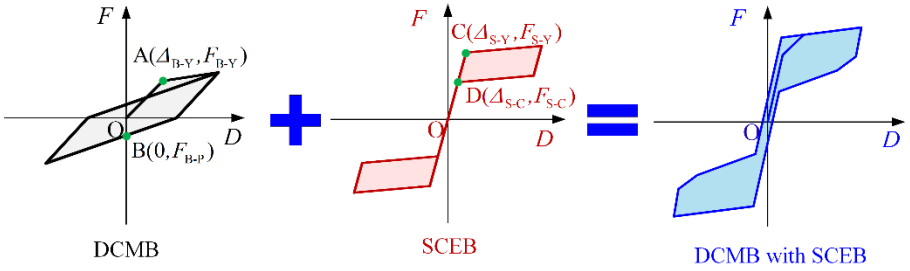

FIGURE 3 Restoring force model of DCMB with SCEBs.

According to the analytical model of DCMB with SCEBs, three critical design philosophies of the SCEBs in DCMB are developed to achieve satisfactory seismic performance:

(1) Based on the structural fuse concept, the SCEB should yield before the bent, which can be expressed as Equation 10:

$$\Delta_{S-Y} \le \Delta_{B-Y-S} \tag{10}$$

in which, Δ_{B-Y-S} is the deformation value of the corresponding SCEB when the bent yields.

Assuming that the cap beam is rigid, the yield displacement of the bent with two circular cross-section columns can be calculated using Equation 11[42]:

$$\Delta_{B-Y} = \frac{\xi}{6}\varepsilon_{ry}\frac{H^2}{D} \tag{11}$$

where ξ is a constant factor between 2.0 and 2.5[42]; ε_{ry} is the yield strain of the longitudinal reinforcement in the column; D is the column diameter; H is the column height.

(2) To obtain the full self-centering capacity, the brace should meet the requirement that the self-centering force in the horizontal component of the SCEB is larger than or equal to the restoring force (at point B) of the bent; the following condition should be satisfied:

$$F_{S-C'} \ge F_{B-P} \tag{12}$$

in which:

$$F_{S-C'} = F_{S-C} \cdot \cos\beta_1 \tag{13}$$

(3) In the design, the deformation capacity of the SCEB should also be considered. The deformation relationships between the bent and SCEBs are shown in Figure 2A. The deformability of SCEBs (ΔS_m) should be larger than that of SCEBs that corresponds to the maximum allowable lateral displacement (X_m) of the bent, which can be expressed as:

$$\Delta S_{1m} \ge \left|\sqrt{(L_1 + X_{1m})^2 + h_1^2} - \sqrt{L_1^2 + h_1^2}\right| \tag{14}$$

$$\Delta S_{2m} \ge \left|\sqrt{L_1^2 + h_2^2} - \sqrt{(L_1 + X_{1m} - X_{2m})^2 + h_2^2}\right| \tag{15}$$

$$\Delta S_{3m} \geq \sqrt{(L_1 + X_m - X_{2m})^2 + h_3^2} - \sqrt{L_1^2 + h_3^2} \tag{16}$$

where X_{1m}, X_{2m} and X_m are respectively the maximum horizontal displacement of NODE1, NODE2, and NODE3, respectively. X_{1m} and X_{2m} can be calculated as:

$$\begin{cases} X_{1m} = h_1 \cdot X_m / H \\ X_{2m} = (h_1 + h_2) \cdot X_m / H \end{cases} \tag{17}$$

3. RC DOUBLE-COLUMN MEDIUM HEIGHT BENT SPECIMENS

A RC DCMB with link beams (with a height of 12 m) from an actual bridge structure was selected, as shown Figure 4B. The SCEB-Us/EDB-Us were applied to the DCMBs in a K-shaped form along the height of the column instead of the traditional link beams, as shown in Figure 4C. Furthermore, a DCMB (without link beam) was also considered as the control specimens. It should be noted that this bare DCMB (with a height of 12 m) is not an actual bridge bent, because the height of a double-column bridge pier exceeding 10 meters requires the installation of the link beam according to the JTG/T 2231-01-20207[46]. Considering the capacity of the loading equipment, four 1:4 scaled bent specimens (including DCMB, DCMB with link beams, and DCMB with SCEBs/EDBs) were designed and manufactured. Figure 4 shows the configurations and the geometric details of the bent specimens. It should be noted that the geometry and reinforcement of the four bent specimens were identical to each other, thus ensuring fair comparisons of the results could be made.

The DCMB specimen included two circular columns, and the diameter of each circular column was 300 mm, and the height was 3000 mm. Eight rebars with a diameter of 12 mm were installed along the column, and the longitudinal reinforcement ratio was 1.28%. The diameter of the stirrup was 6 mm, and the space between adjacent stirrups was 75 mm, which resulted in a transverse reinforcement ratio of 0.6%. The concrete cover was 25 mm. The width and height of the link beam cross-section were 240 mm and 300 mm, respectively. There were four longitudinal rebars with a diameter of 10 mm, equally distributed in the cross-section of the link beam. The cross-section of the square cap beam was 400 mm × 400 mm, and the length was 2600 mm. Figures 4D-E show the cross sections of the column and the cap beam, respectively.

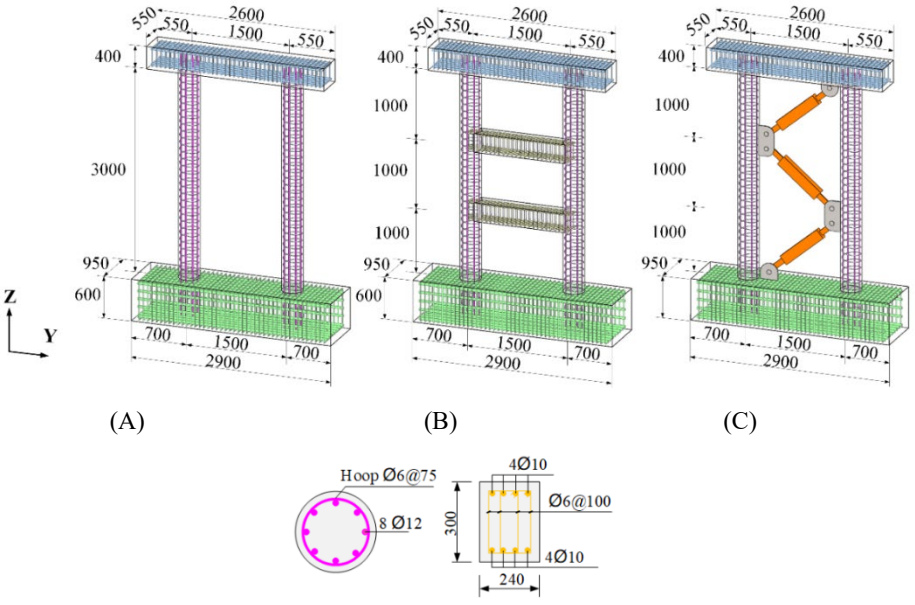

FIGURE 4 Details of the bridge bent specimens (unit: mm) (A) DCMB; (B) DCMB with link beams; (C) DCMB with SCEB-Us/EDB-Us; (D) cross-section of the column; (E) cross-section of the link beam.

C40 concrete was used for the bridge bents. The uniaxial compressive strength of the concrete at 28 days was tested, and the average strength was 50.37 MPa. HRB400 reinforcement bars, with a design yielding strength of 400 MPa, were used for the longitudinal rebars and the stirrups. The yielding strength, ultimate strength, and ultimate strain of the rebars were also obtained from tests, and the average values were 392 MPa, 498 MPa, and 16%, respectively.

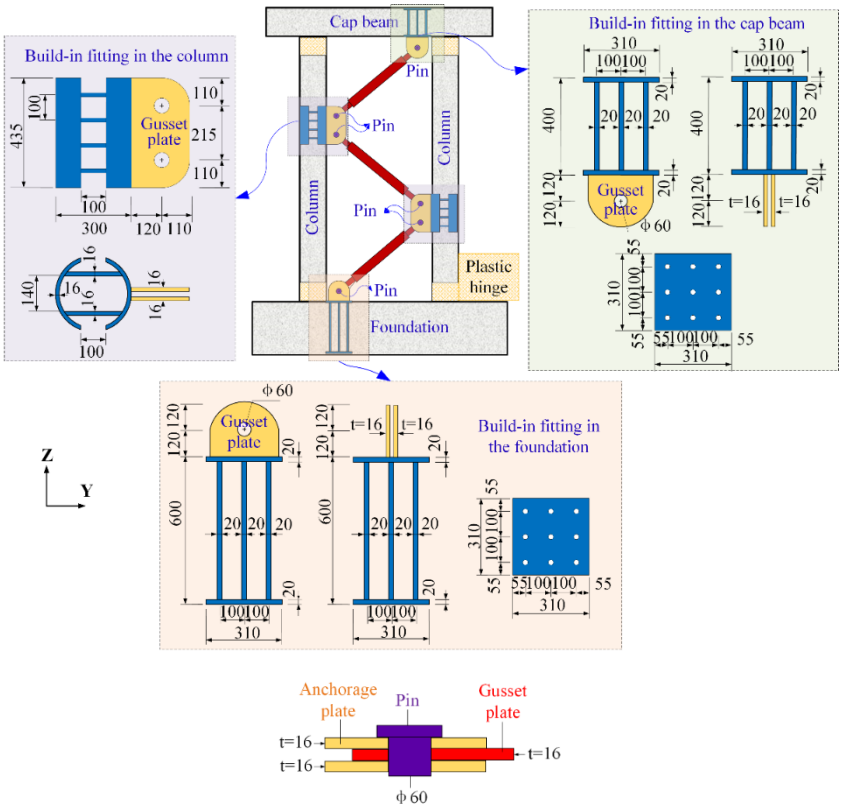

FIGURE 5 Bent-brace connection details (unit: mm).

Q345 steel with a yielding strength of 345 MPa (f_y=345 MPa) was selected for the anchorage plates, and #45 (f_y=355 MPa) steel was selected for the pin. Figure 5 shows the bent-brace pin connection details. To satisfy the strength requirements, the thickness of the anchorage plate was t=16 mm, and the diameter of the pin was d_0=60 mm.

4. DESIGN AND PERFORMANCE OF THE SCEB-U

The SCEB was designed according to the three design philosophies mentioned previously (in Sect. 2.2). The restoring force and yield displacement of the DCMB were calculated as 25 kN and 20 mm, respectively. Thus, the axial self-centering force and yield displacement of the brace can be calculated as 29.8 kN ($25\ kN/\cos\beta_1$) and 5.6 mm, respectively, according to Equations 12-17. To consider a safety factor, 40 kN is taken as the self-centering force of the SCEB.

In the experimental test, the same loading protocol was adopted to investigate the whole performance level of the DCMB, DCMB with link beams, DCMB with EDBs, and DCMB with SECBs, and the maximum displacement drift ratios were set as 5%[48]. When the deformation of the DCMB is 150 mm (the corresponding drift ratio is 5.0%), the maximum deformation of the brace should be larger than 42 mm, according to Equations 1-3 in Sect. 2.2. It is worth noting that the BRB was originally chosen as the primary choice for energy-dissipating element for SCEB. However, the deformation capacity of the BRB is normally 3% of the working section[49], which does not satisfy the allowable deformation of the braces arranged in the bridge bent. In order to satisfy the deformation of the SCEB in

this study, the U-shaped plate was chosen as the energy dissipation element, while the combination disc spring was selected as the self-centering element. In this study, U-shaped plates brace as the pure energy dissipation brace was also considered. For a fair comparison, the yield force of the EDB-U is designed to be equal to that of the SCEB-U.

4.1 DESIGN OF EDB-U AND SCEB-U SPECIMENS

Figure 6 shows the configuration of the SCEB-U and EDB-U system. As shown in Figure 6A, the EDB-U mainly consists of some U-shaped steel plates, an outer tube, a piston plate, and a group of high-strength bolts. The U-shaped steel plates are bolted between the outer tube and the piston plate as energy-consuming (ED) components. When the EDB-U is under tension or compression, relative movement occurs between the piston plate and outer tube, which deforms these U-shaped plates, resulting in energy dissipation.

Figure 6B shows the configuration of SCEB-U. It can be seen that the SCEB-U consists of a traditional energy dissipation (ED) system and a self-centering (SC) system. U-shaped steel plates are used as ED components in the SCEB-U. The SC system is offered by the combined disc springs, and the combined disc springs are prepressed to the target deformation by the block plates. The piston plate passes throughout the prepressed disc springs; thus, the deformations of the combined disc springs and U-shaped steel plates are always consistent. The assembly manner can facilitate inspection and replacement of the damaged elements after strong earthquakes, if necessary.

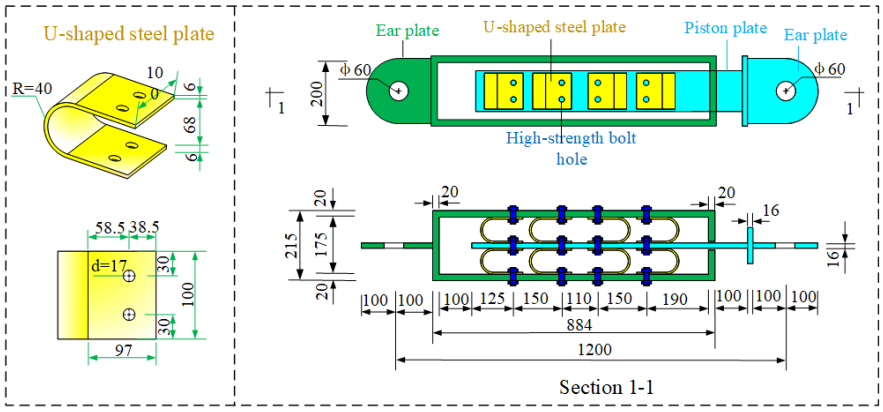

(A)

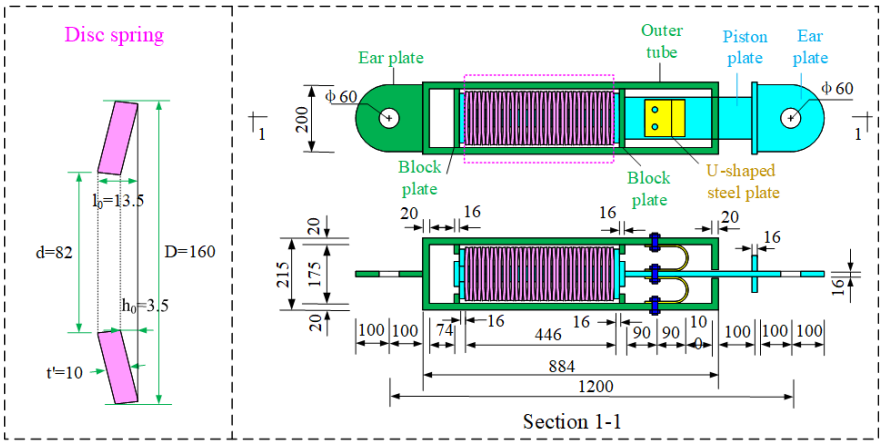

(B)

FIGURE 6 Configuration and dimension (unit: mm) of EDB-U and SCEB-U (A) EDB-U; (B) SCEB-U.

Figure 6 shows the large-scale specimens of the EDB-U and SCEB-U. The specimens have a global length of 1400 mm and a cross-section of 215 mm × 200 mm. The straight segments of the U-shaped steel plates are bolted with the piston plate and outer tube by using high-strength bolts with grade 10.6 M16. For EDB-U and SCEB-U, all the U-shaped steel plates are made of Q235 steel, and Q345 is used in the manufacturing of other parts. The

dimensions of U-shaped steel plates are shown in Figure 6A; each one has a height of H = 80 mm, a total length of L = 100 mm, a radius of R = 40 mm, and a plate thickness of t = 6 mm. The deformation capacity of the U-shaped plate is 100 mm.

For SCEB-U, the disc springs made of 60Si2MnA steel are selected according to the Disc Spring Standard (GB T1972–2005 [50]), as shown in Figure 7C. For each disc spring, the outer diameter is D = 160 mm, the inner diameter is d = 82 mm, the thickness is t′ = 10 mm, the free height is H_0 = 13.5 mm, and the maximum compression deformation is H_0' = 3.5 mm. A total of 36 disc springs are used for the brace, with a total maximum permissible deformation of 126 mm. For SCEB-U, the deformations of the combined disc springs and U-shaped steel plates are always consistent. The deformation capacity of the braces is much greater than the required value (42 mm). To provide the SC capability to the system, the pre-compressive disc springs are kept in the compressed condition at all times, and the initial pre-pressure of the disc spring is set as 60 kN according to Equations 12-13.

4.2 HYSTERETIC PERFORMANCE OF EDB-U AND SCEB-U SPECIMENS

To investigate the hysteretic behavior of the SCEB-U and EDB-U systems, quasi-static cyclic tests were performed in the State Key Laboratory of Bridge Engineering Safety and Resilience at the Beijing University of Technology (BJUT), China. A series of cyclic loading tests of the two braces were conducted on the 3000 kN servo hydraulic test system, as shown in Figure 7, and the tests employed a displacement-control loading scheme with two cycles at each target deformation, as shown in Figure 8A.

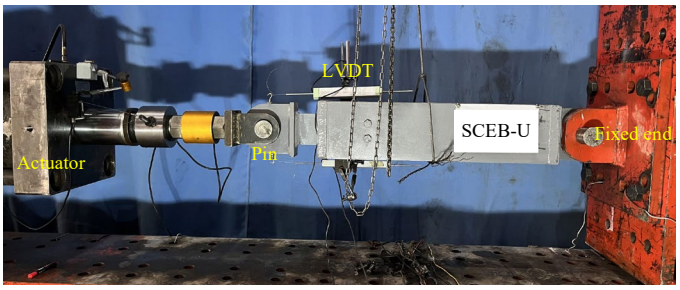

FIGURE 7 Photo of the testing setup.

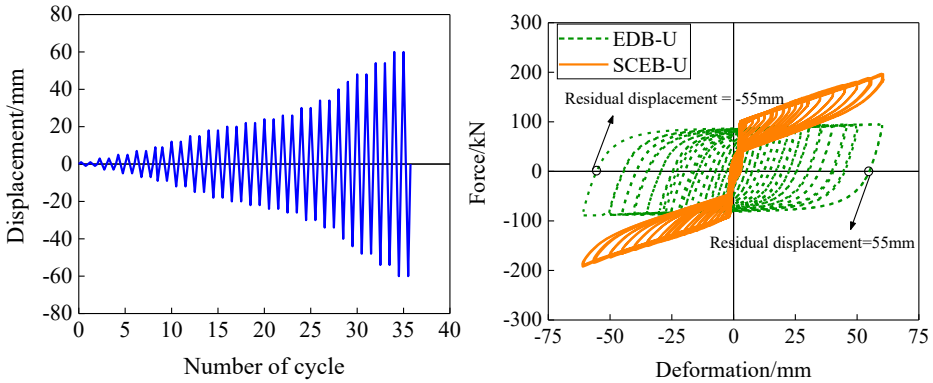

(A) (B)

FIGURE 8 (A) Loading protocol for brace specimens and (B) hysteresis curves of the SCEB-U and EDB-U.

Figure 8B presents the hysteretic curves of the EDB-U and SECB-U specimens. As shown in Figure 8B, the EDB-U exhibited full and stable energy dissipation capacity without obvious stiffness and strength degradation. The yield displacement of EDB-U was 5.0 mm, which was smaller than the required value (5.6 mm) as mentioned before. The yield force and the peak force were 78 kN and 95 kN. Notably, the deformation capacity of EDB-U reached 60 mm, which was significantly greater than the 42 mm needed for the design (Sect. 2.2). However, the EDB had a

very significant residual displacement of up to 55 mm (residual displacement ratio = 4.6%) when the ultimate displacement of 60 mm was applied.

SCEB-U exhibited typical flag-shaped hysteresis curves with stable energy dissipation ability and excellent self-centering capability, as shown in Figure 8B. Identical to EDB-U, the yield displacement (3.1 mm) of SCEB-U was smaller than the required value (5.6 mm), which satisfied the design philosophies in Sect. 2.2. In particular, when the deformation of SCEB-U reached 60 mm, the residual displacement of SCEB-U was only 2.8 mm, which was much smaller than that (55 mm) of EDB-U. It was found that the yield force of the SCEB-U was close to that of the EDB-U, which is consistent with the previous design.

5. QUASI-STATIC TESTS OF THE BENT SPECIMENS

5.1 TEST SETUP

Figure 9 shows the schematic drawing of the test setup of the RC DCMB specimens. As shown, one actuator was installed horizontally to provide the cyclic load to the specimen top, and two hydraulic jacks were used to provide the vertical load. In the present study, the vertical load provided by the two jacks was 15% of the axial load carrying capacity of the column, i.e., $0.15 f_c^{'} A_g$ [51], where $f_c^{'}$ is the concrete compressive strength and A_g is the gross section area of the column. The vertical load provided by each jack was therefore 200 kN, based on the information provided in Sect. 4.1. Linear variable displacement transducers (LVDTs) were installed at different heights of the column to measure the lateral displacement of each column, as shown in Figure 9. The axial deformation of the brace was measured by pull-line displacement sensors installed in parallel with the brace.

The seismic behavior of the four bridge bents under the cyclic loading was tested in the present study, as shown in Figure 11, and Figure 10 shows the loading protocol. In order to compare the damage mode and hysteresis performance of different bents under different loading amplitudes, these tests were conducted using a uniform displacement-controlled loading protocol, and two cycles were applied at each lateral displacement level.

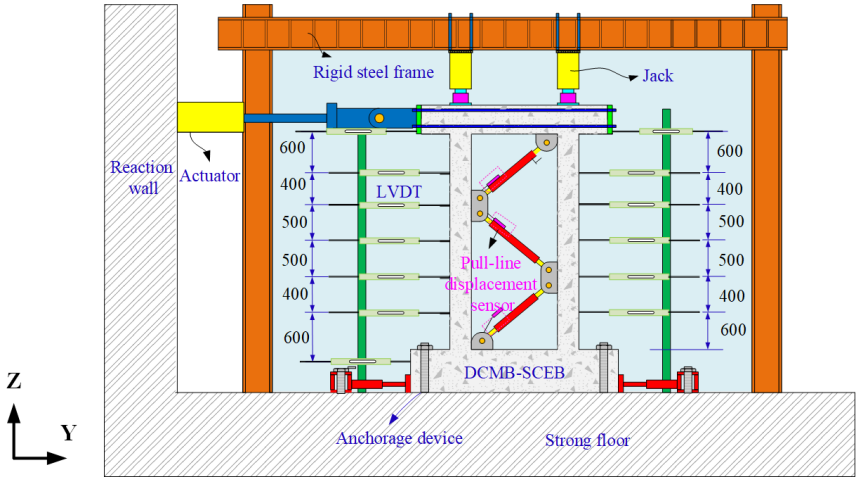

FIGURE 9 Schematic drawing of the test setup of specimens

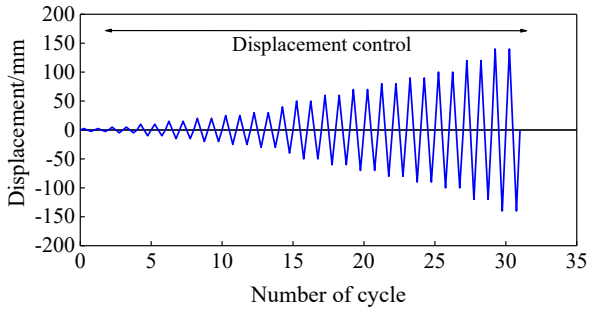

FIGURE 10 Loading protocol for the bent specimen.

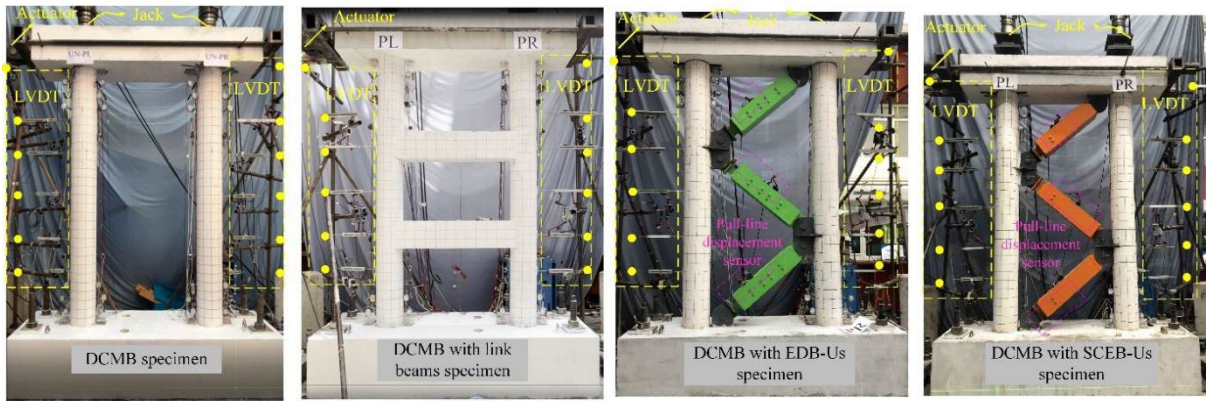

FIGURE 11 Pictures of test setup for DCMB, DCMB with link beams, and DCMB with SCEB/ EDB.

5.2 EXPERIMENTAL RESULTS

5.2.1 DAMAGE PATTERNS

The damage patterns of the four specimens are displayed in Figure 12. In the present study, the specimens are considered as failed when the lateral strength is smaller than 85% of the maximum strength. It is important to note that the DCMB with link beams was the primary comparison specimen with the DCMB with SCEB-Us/EDB-Us. The DCMB was mainly used to obtain the hysteretic performance of the bare bent, which is used to design for attaching SCEB-Us and EDB-Us to the DCMB.

Figure 12A shows the damage pattern of DCMB after the test. As shown, the damaged regions were mainly focused on the top and bottom of the columns. It was found that severe crushing and spalling of concrete appeared at the top and bottom of the columns. The buckling of the reinforcement and the stirrups at the top and bottom of the column were observed. As will be shown in the hysteretic curve, when the bent top displacement reached 130 mm (DR = 4.30%), the strength reduced to 82 kN (85% of the maximum strength), which can be considered failed.

Figures 12B-C present the damage pattern of DCMB with link beams after the test. It is found that the link beam-column joints are also severely damaged, in addition to the top and bottom of the columns. Severe crushing and spalling of concrete appeared at the link beam-column joints. The concrete core at the two ends of the link beams was broken, and the fracture of the reinforcement and buckling of the stirrups were also observed. As can be seen from Figure 14B, the strength significantly fell to 154 kN (85% of the maximum strength) when the bent top displacement reached 90 mm (DR = 3.00%). Compared with DCMB, the DCMB with link beams failed earlier.

As can be seen from Figure 12D-E, the damage areas of DCMB with SCEB-Us/EDB-Us mainly focused on the top and bottom of the two columns. It's worth noting that there was no obvious damage in the regions around the brace-column joints, which is consistent with the force analysis in Sect. 2 that the horizontal force components of the two braces acting on the same column-brace joint can cancel each other out. Moreover, the horizontal

components of the axial force of the top brace and bottom brace were transferred to the cap beam and the foundation, respectively. There was no obvious damage to the cap beam or foundation. It is verified that this connection between the braces and the bent can maximize the protection of the columns from damage. The damage of the DCMB with SCEB-Us/EDB-Us was significantly lighter compared to the DCMB with link beams. It is worth noting that the SCEB-U and EDB-U as structural fuses enter the yield state first to dissipate energy to reduce structural damage and thus protect the columns in the bent, but may not be able to completely avoid damage to the bent. For DCMB with EDB-Us, when the bent top displacement reached 120 mm (DR=4.00%), the force of the specimen fell to 85% of its peak force.

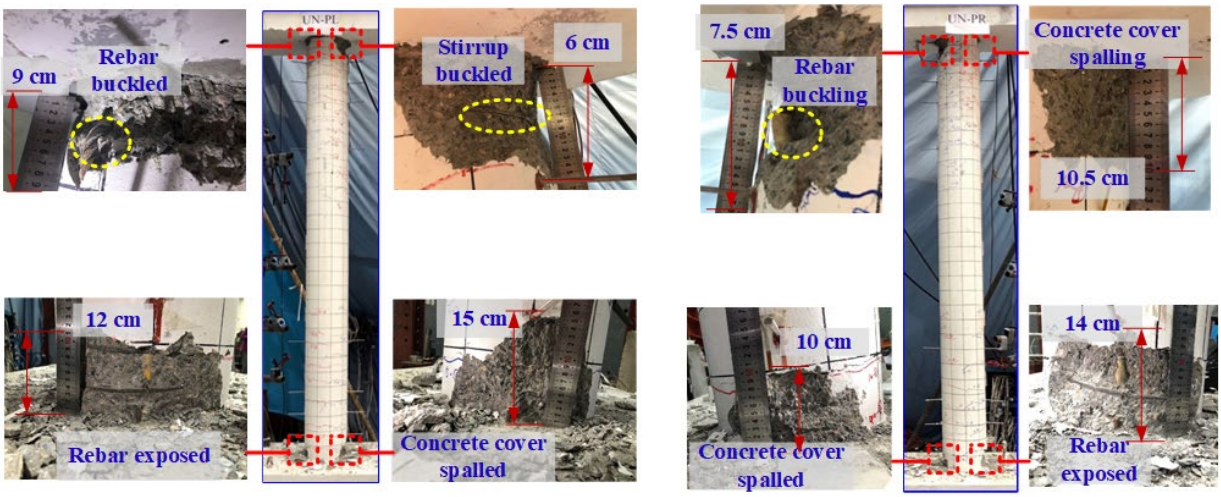

(A)

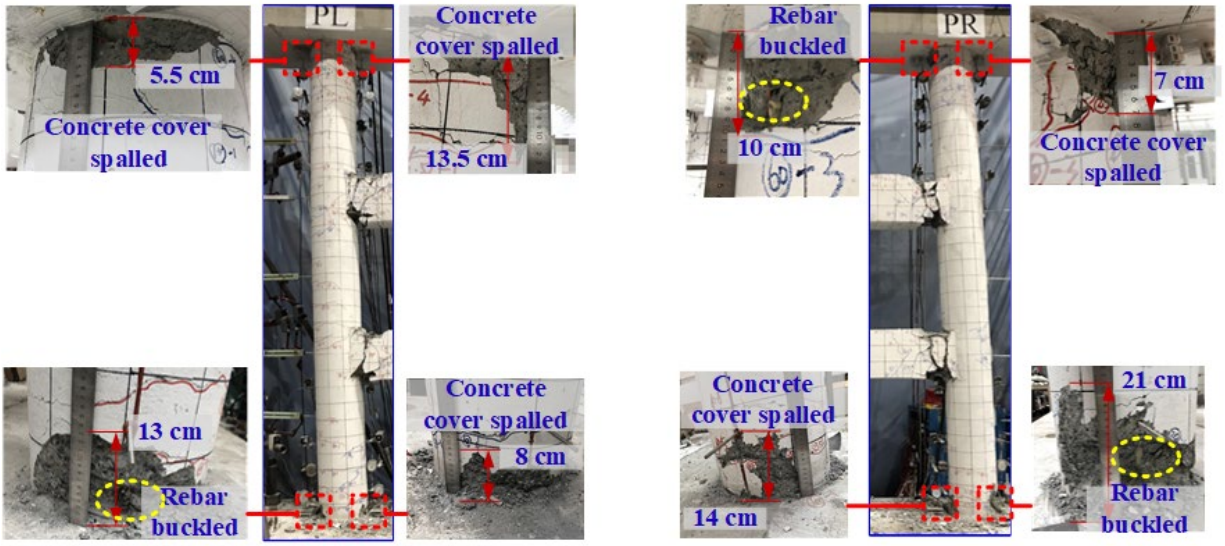

(B)

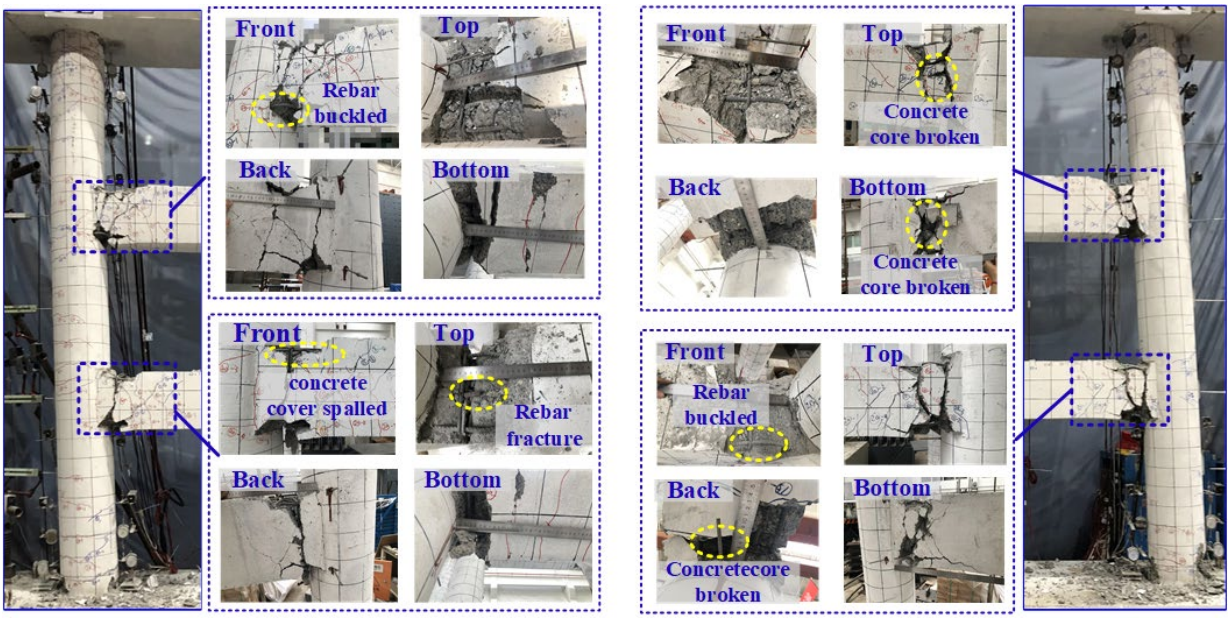
Front
Rebar buckled
Top
Back
Bottom
Front
concrete cover spalled
Top
Rebar fracture
Back
Bottom
Front
Top
Concrete core broken
Back
Bottom
Concrete core broken
Front
Rebar buckled
Top
Back
Concretecore broken
Bottom

(C)

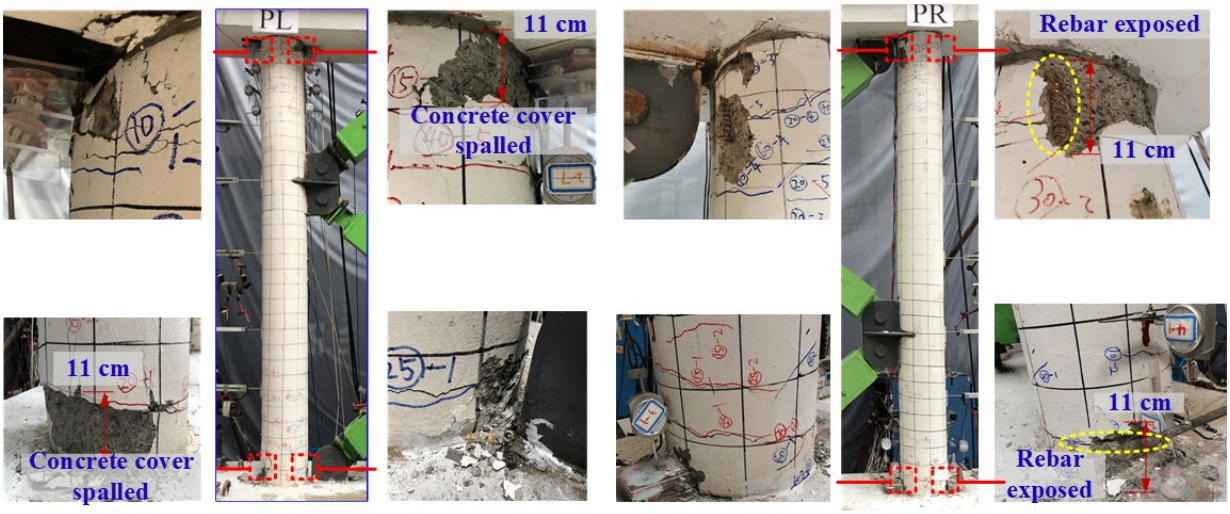
PL
11 cm
Concrete cover spalled
11 cm
Concrete cover spalled
PR
Rebar exposed
11 cm
11 cm
Rebar exposed

(D)

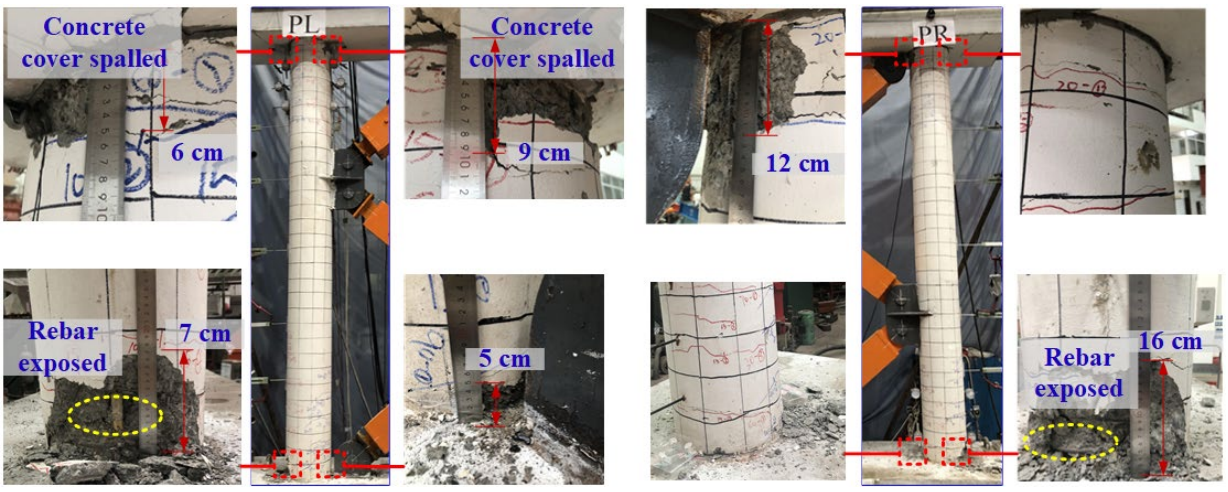
Concrete cover spalled
6 cm
PL
Concrete cover spalled
9 cm
12 cm
PR
Rebar exposed
7 cm
5 cm
Rebar exposed
16 cm

(E)

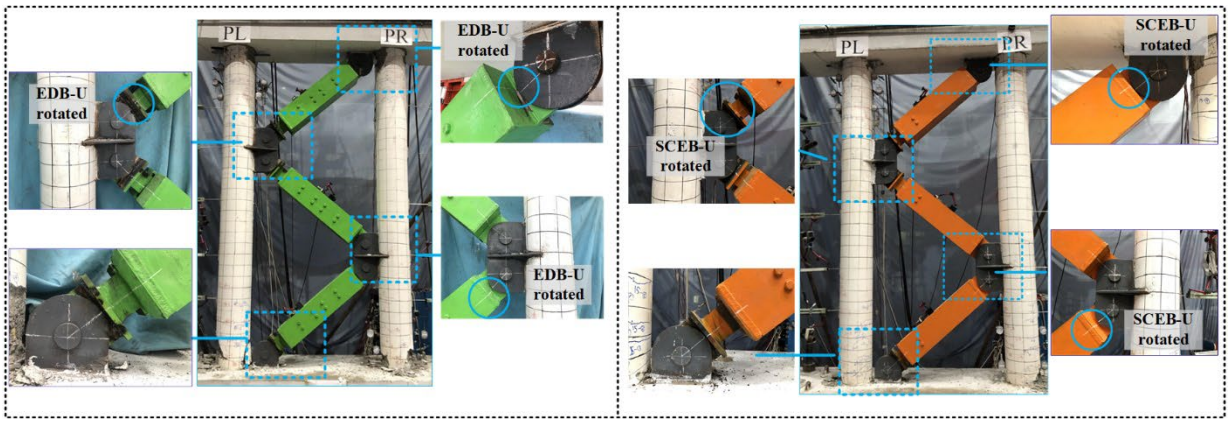

(F)

FIGURE 12 Damages of (A) DCMB; (B-C) DCMB with link beams; (D) DCMB with EDBs; (E) DCMB with SCEBs; (F) column-brace connection regions of DCMB with EDB-Us/SCEB-Us.

Figure 13 shows the deformation curves of EDB-Us and SCEB-Us in bents during tests. As can be seen from the figure, when the bent was subjected to a positive load, EDB-U1/SCEB-U1 and EDB-U3/SCEB-U3 underwent tensile deformation, and EDB-U2/SCEB-U2 underwent compressive deformation. When the bent was subjected to the negative load, EDB-U1/SCEB-U1 and EDB-U3/SCEB-U3 underwent compressive deformation, and EDB-U2/SCEB-U2 underwent tensile deformation. These phenomena were consistent with the force analysis in Sect. 2.1. In particular, the maximum deformation of the brace reached 46 mm.

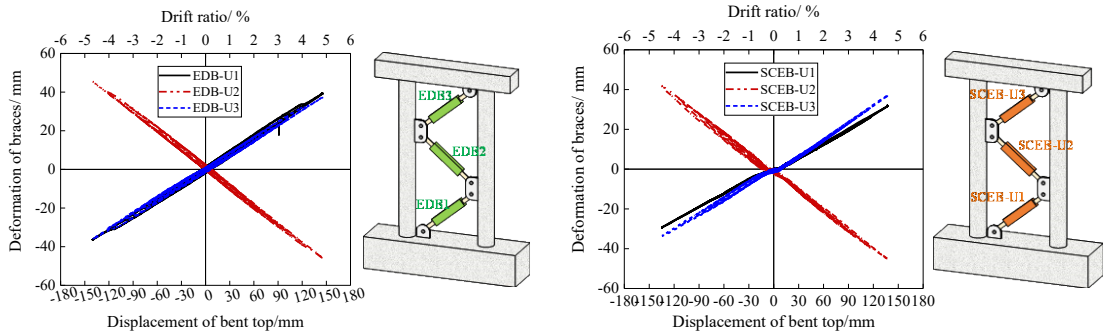

(A)

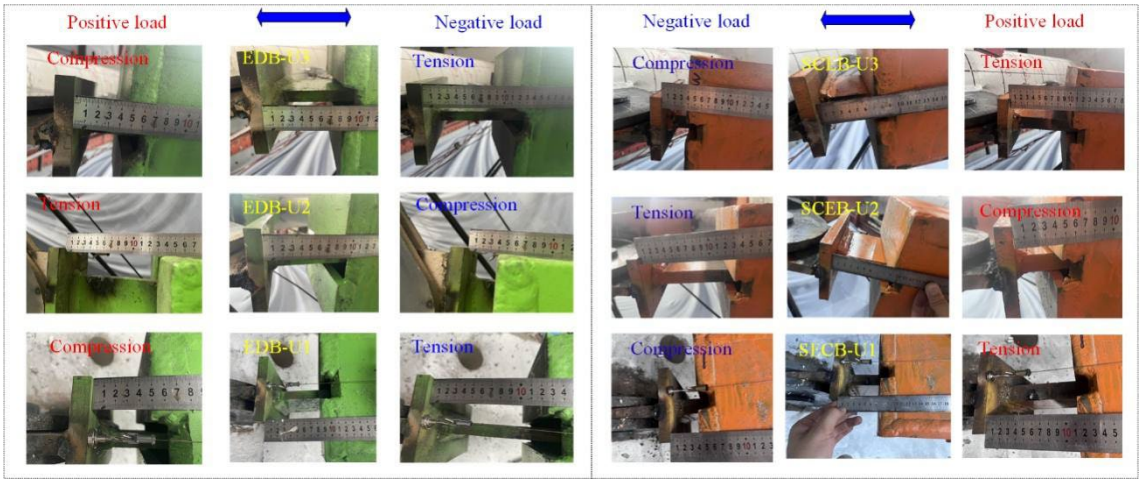

(B)

FIGURE 13 (A) Deformation curves of braces (EDB-Us and SCEB-Us); (C) deformation pictures so braces (EDB-Us and SCEB-Us).

Figure 14 displays the final deformation mode of the EDB-U and SCEB-U when the tests of the DCMB with

EDB-Us/SCEB-Us were completed. As can be seen from the figure, relative displacement occurred between the bolts along the EDB-U axis., i.e., residual deformation existed in the EDB. In particular, there was almost no relative displacement between the bolts in SCEB, i.e., there was no residual deformation in SCEB.

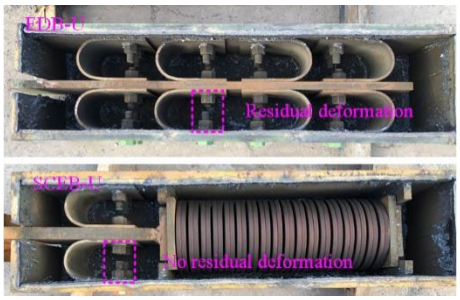

FIGURE 14 Final deformation mode of EDB-U and SCEB-U.

5.2.2 HYSTERETIC BEHAVIOR

Figure 15 shows the lateral force-displacement relationship curves of DCMB, DCMB with link beams, DCMB with EDB-Us, and DCMB with SCEB-Us. The critical parameters of hysteretic curves of DCMB, DCMB with link beams, DCMB with EDB-Us, and DCMB with SCEB-Us are listed in Table 1. The natural period of the DCMB with SCEB-Us was calculated to be 0.30 s, which is slightly larger than that of the DCMB with link beams (0.28 s).

As shown in Figure 15A, DCMB represented shuttle-shaped hysteretic behavior. The hysteretic curves of the DCMB were plump and with obvious stiffness and strength degradation due to the severe concrete crushing and rebar buckling at the top and bottom of the columns, as shown in Figure 15A. It was found that the DCMB began to yield at the bent top displacement of 21.2 mm (DR=0.93%), and the corresponding (yield) force was 73.7 kN. The strength of the bent reached the maximum value (97.3 kN) when the bent top displacement was 60 mm (DR = 2.00%). After that, the strength decreased gradually due to the damage to the concrete and rebars. At the bent top displacement of 140 mm (DR=4.67%), the strengths reduced to 76 kN and -68.9 kN in the directions of positive and negative displacement, respectively. In particular, a large residual displacement existed in the bent after the test. When a bent top displacement of 140 mm was applied to the bent specimen, the residual displacements in the negative and positive displacement directions were, respectively, 90.88 mm and 86.78 mm, as shown in Figure 15A.

According to Figure 15B, the hysteretic curves of the DCMB with link beams showed a shuttle shape. Compared with that of DCMB, there was more significant stiffness and strength degradation. This is due to the fact that the DCMB with link beams has very severe damage at the column-beam joints, in addition to damage at the bottom and top of the column. The yield displacement of DCMB with link beams is 14.7 mm and 30% smaller than that of DCMB. The yield force and peak force were 136.1 kN and 181.5 kN, and 84.8% and 86.5% greater than that of DCMB, respectively. Then, the strength of the bent specimen quickly diminished, and the strength decreased to 63% and 57% of its maximum strength when the bent top displacement reached 140 mm (DR = 4.67%) and -140 mm. In particular, a large residual displacement existed in the bent after the test. The residual displacements were 90.78 mm (3.0%) and 99.61 mm (3.3%) in the positive and negative displacement directions, respectively, after a displacement of 140 mm was applied to the specimen, as seen in Figure 15B. The displacement ductility factor of DCMB with link beams was nearly equal to that of DCMB, indicating that the ductility of the bents was not enhanced by the link beams.

Compared with the DCMB with link beams, the DCMB with EDB-Us or SCEB-Us has better bearing capacity, energy dissipation capacity, and a larger displacement ductility factor, as shown in Figure 15. The yield displacements of the EDBs (5.0 mm) and SCEB-Us (3.1 mm) were smaller than the required value (5.6 mm), as mentioned before. This means that more energy may be dissipated by the EDBs or SCEBs, protecting the RC bent. As shown in Figure 15C, DCMB with EDB-Us behaved shuttle-shaped hysteretic behavior, and strength

degradation can be observed. The stiffness and strength of the retrofitted bents degrade mainly because the stiffness and strength of the bare bent decrease. The maximum force of the bent was 205.9 kN (13.4% increase over DCMB with link beams) when the bent top displacement was 50 mm (DR = 1.67%). It is observed that a large residual displacement occurred in the DCMB with EDB-Us after the test. The residual displacement of the DCMB with EDB-Us was around 110 mm at a bent top displacement of 140 mm, which is 21% bigger than that of DCMB with link beams. The primary reason for this issue is that both the bent and the EDBs have been left with substantial residual deformations.

The lateral load-deformation hysteretic curves of the bent with SCEB-U are shown in Figure 15D. It can be seen that the bent with SCEB-Us exhibited a flag-shaped hysteretic curve with good SC capability. The strength and stiffness of the bent with SCEB-Us increased significantly compared to the case with EDB-Us. For example, the peak force (249.5 kN) of DCMB with SCEB-Us increased by 37.4% over DCMB with link beams and 21.2% over DCMB with EDB-Us. It should be noted that the strength continued to increase instead of decreasing after yielding; thus, the ultimate displacement was taken as the bent top displacement at the end of loading (140 mm). The strength and stiffness of the DCMB with SCEB-Us approximately equal the sum of the strength and stiffness of the DCMB and SCEB-U1, which is consistent with the previous analysis. The yield strength (161.5 kN) of the DCMB with SCEB-U is approximately equal to the sum of the strength of the DCMB (66 kN) and the horizontal force components of SCEB-U (90.7 kN=108 $kN \cdot cos\,\beta_1$) at the corresponding DCMB with SCEB-U yield displacement. Specifically, the residual displacement was minimal, measuring only 9.8 mm (0.33%) in the positive direction and 13.5 mm (0.45%) in the negative direction when the ultimate bent top displacement of 140 mm (DR = 4.67%) was applied. It is noteworthy that the residual displacement of the DCMB with the SCEB-Us is much smaller than that of the DCMB with link beams. This demonstrates the effectiveness of applying SCEB-U as an alternative to RC link beams in reducing the residual displacements of DCMB with link beams.

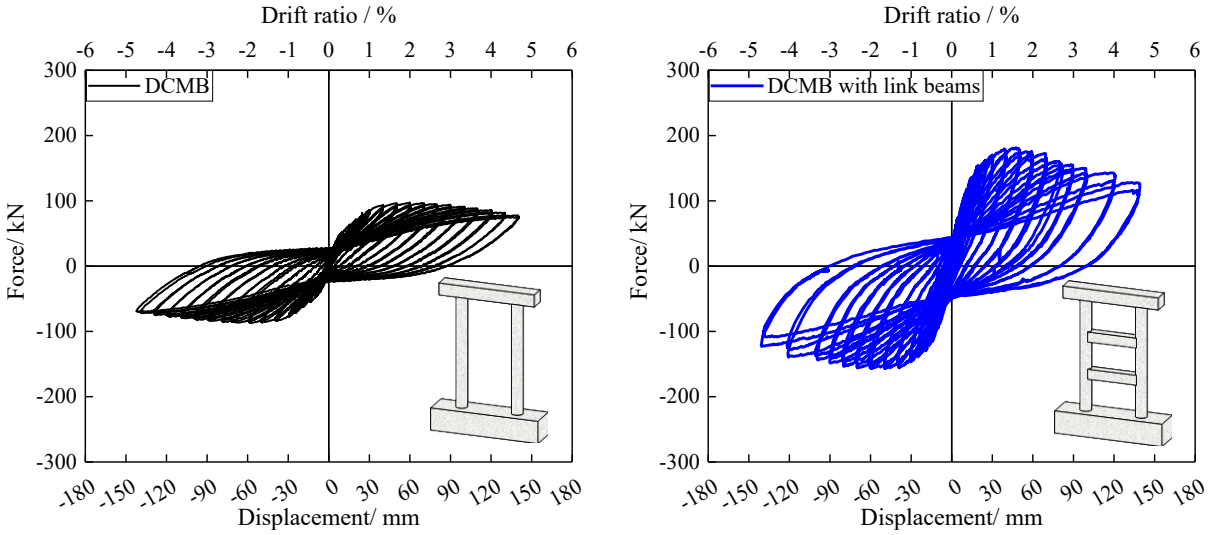

(A) (B)

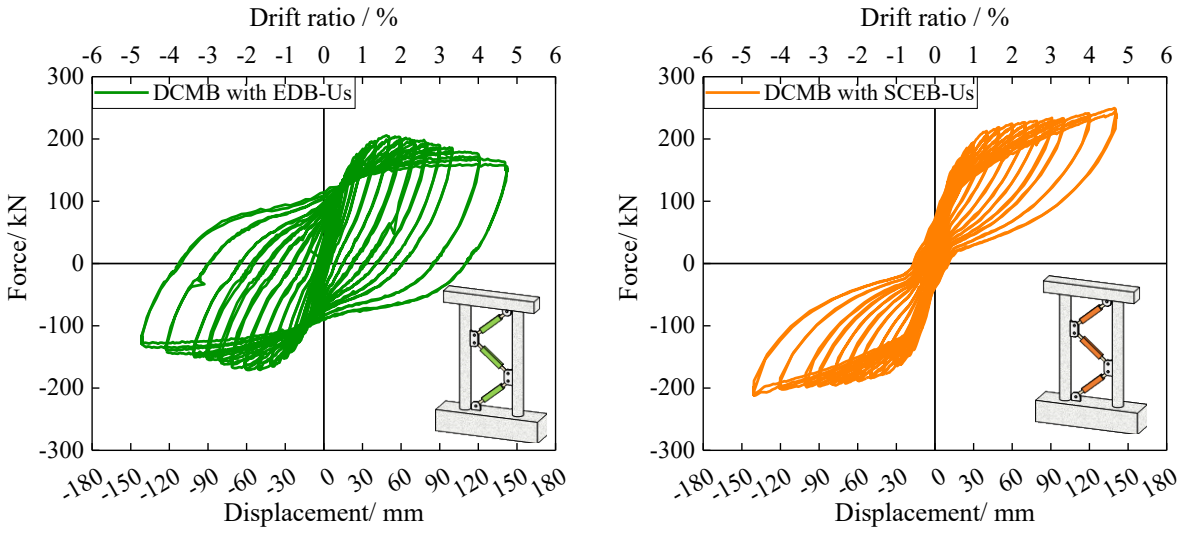

(C) (D)

FIGURE 15 Hysteretic curves of :(A) DCMB; (B) DCMB with link beams; (C) DCMB with EDBs; (D) DCMB with SCEB-Us

Table 1 Comparison of the seismic behavior of the four bents under cyclic loads

Model	Initial stiffness (kN/mm)	Yield force (kN)	Yield displacement (mm)	Peak force (kN)	Ultimate displacement (mm)	Displacement ductility factor
DCMB	12	73.7	21.2	97.3	130	6.1
DCMB with link beams	23	136.1	14.7	181.5	90	6.1
DCMB with EDB-Us	20	145.9	15.6	205.9	120	7.7
DCMB with SCEB-Us	22	161.5	15.0	249.5	140	9.3

Note: the yield strength, yield displacement, and displacement ductility factor in the table are obtained by the geometric graphic method[43].

5.2.3 CURVATURE

The column curvatures were calculated using the displacements measured by the displacement transducers located along the columns. The curvatures that in this case represent the curvature along the vertical distance between the transducers were derived from rotation, which was computed by dividing the algebraic summation of the relative displacements between opposite transducers at the same height by the horizontal distance between them, as shown in Figure 16. The average curvature for the segment was calculated using Equation 18

$$\phi = \frac{(h_t - h) - (h_c - h)}{h(D + d_t + d_c)} \tag{18}$$

where ϕ is the experimental curvature of the section, the gauge length h is the length of the segment under consideration, and D is the diameter of the column section. The variables d_t and d_c are the clear distances of the instruments from the surface of the column.

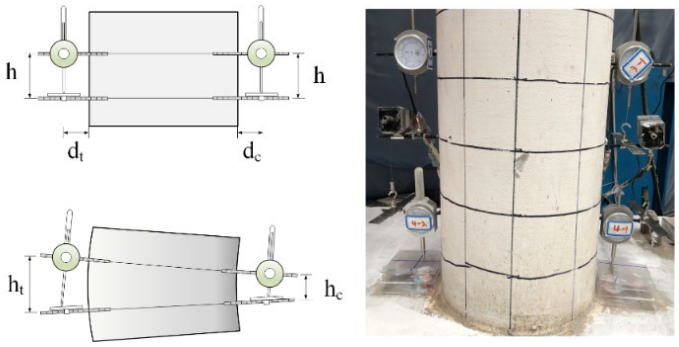

FIGURE 16 Instrumentation setup for measurement of average curvatures on a segment of columns.

Besides, only the curvature at the top of the left column and the bottom of the right column for the different specimens were presented, because the curvature of DCMB with SCEB-Us and DCMB with EDB-Us cannot be measured due to the arrangement of the gusset plate of the built-in fitting.

The yield curvature can be calculated as[53]:

$$\phi_{yc} = \frac{2.25\varepsilon_y}{D} \tag{19}$$

where ε_y is the yield strain of the longitudinal reinforcement, D is the column diameter.

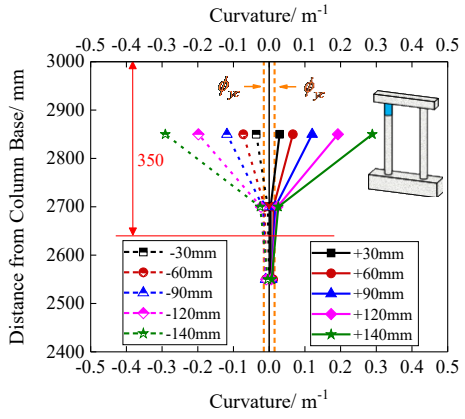

(A)

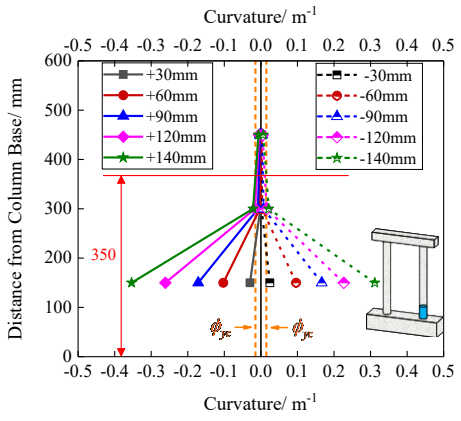

(B)

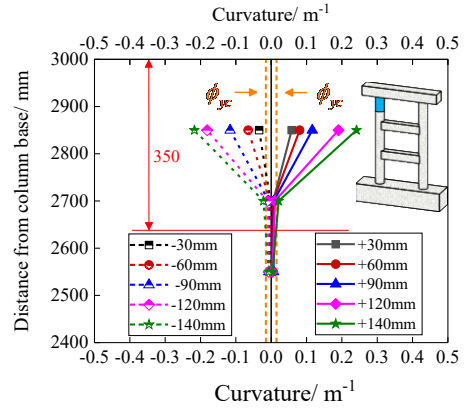

(C)

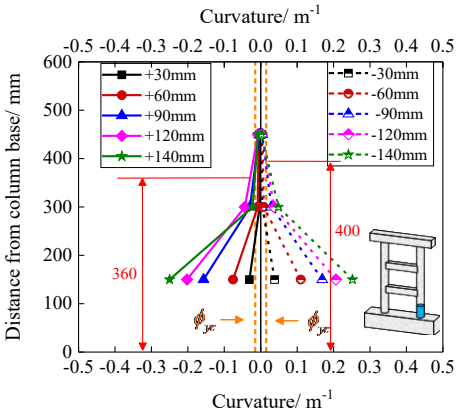

(D)

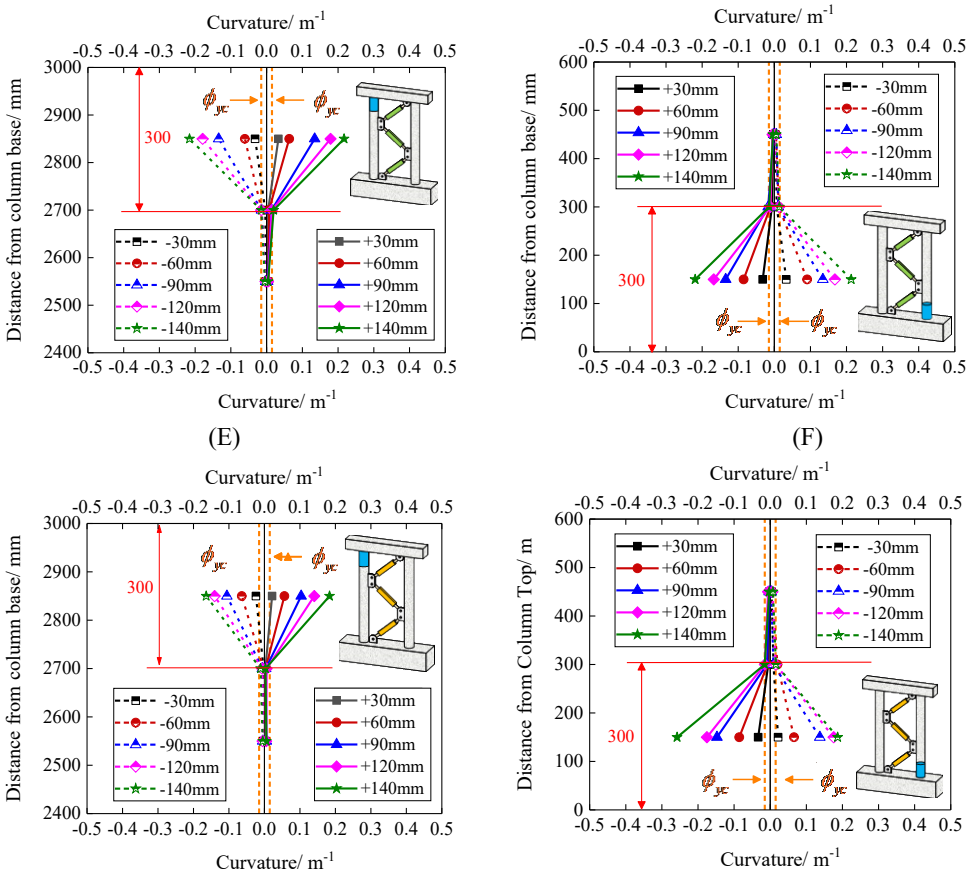

FIGURE 17 Curvature profiles in columns (A) left column of DCMB; (B) right column of DCMB; (C) left column of DCMB with link beams; (D) right column of DCMB with link beams; (E) left column of DCMB with EDB-Us; (F) right column of DCMB with EDB-Us;(G) left column of DCMB with SCEB-Us; (H) right column of DCMB with SCEB-Us

Figure 17 presents the curvature and plastic hinge regions of the four bent specimens. For the four specimens, all the column curvatures exceeded the computed yield curvature values. This result shows that SCEB/EDB can reduce the maximum curve of columns. The regions where the curvature of the column is greater than the yield curvature are considered to be the plastic hinge region. As can be seen from the figure, the plastic hinge regions of DCMB with SCEB-Us/EDB-Us are smaller than those of DCMB and DCMB with link beams, which is consistent with the damage pattern in Sect. 5.2.1. These results indicate that SCEB/EDB designed specifically can indeed limit the damage of the bent.

5.2.4 DRIFT RATIO SHAPE CURVES AND RESIDUAL DRIFT RATIO

Figure 18 shows the deformation shape curves along each column of the four bent specimens. The deformation curves along the column present an inverted triangle, and the deformation increases approximately linearly, even in large deformations. This verifies the correctness of the assumptions made in the simplified analytical model in Sect. 2.1.

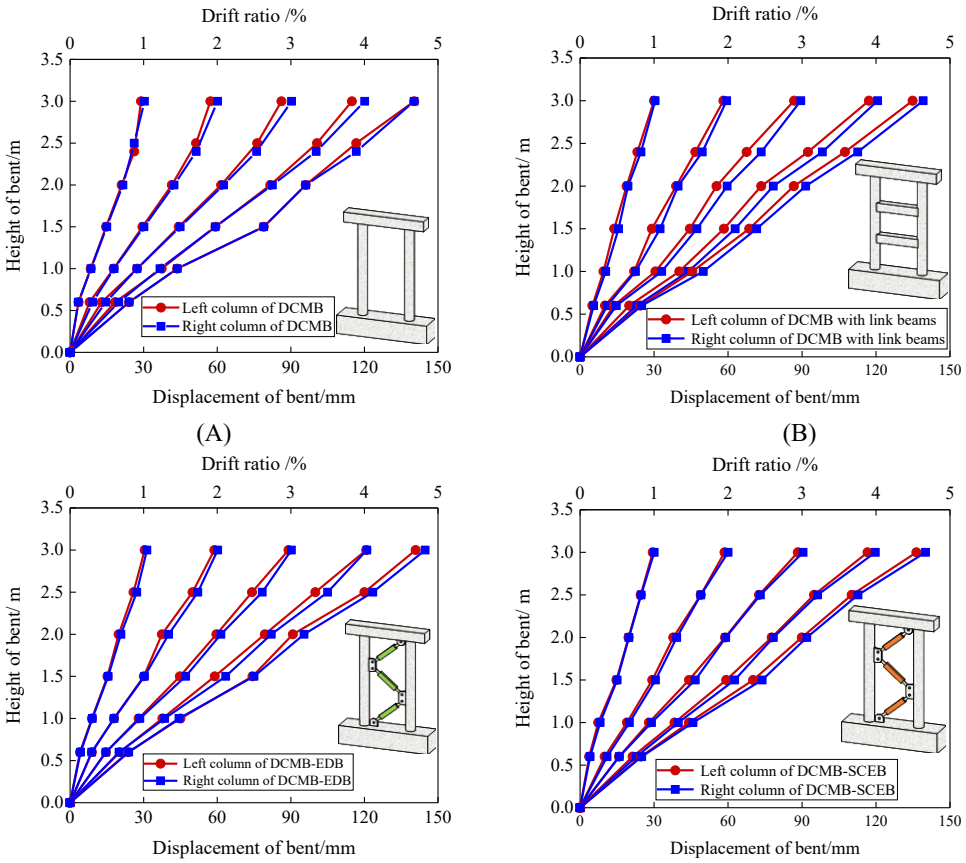

FIGURE 18 Deformation shape curves of columns for (A) DCMB; (B)DCMB with link beams; (C)DCMB with SCEB-Us; (D) DCMB with EDB-Us.

The residual drift ratio, which was defined as the ratio of the residual displacement to the height of the structure, is an important index for estimating the seismic performance and functionality of a structure[48]. According to the suggestion proposed by Erochko et al.[48], when the residual drift ratio is larger than 1.0%, the structure must be strengthened or reinforced at the deformed positions, and when the residual drift ratio is less than 0.5%, no intervention is required.

Figure 19A illustrates the residual drift ratios of the four bents at different drift levels. It can be seen that the residual drift ratio increased with the increment of the structural displacement. DCMB with EDBs resulted in the largest residual drift ratio, followed by the DCMB with link beams and DCMB. The SCEB-Us system provided excellent SC capability to the bent and resulted in the smallest residual drift ratio.

As shown, the residual drift ratios of the DCMB, DCMB with link beams, and DCMB with EDB-Us were larger than 1.0% when the ultimate bent top displacement of 140 mm (DR=4.6%) was applied. The bent lost its functionality according to the criteria given by Erochko et al.[48]. When the SCEB-Us systems were installed in the bent, the residual drift ratios decreased dramatically to below 0.5%, indicating the bridge bent was functional after the earthquake event. The results clearly demonstrate the effectiveness of applying SCEB-Us to reduce the residual displacement of the DCMB with link beams.

5.2.5 STIFFNESS DEGRADATIONS

Stiffness degradation is an important property of RC bridges subjected to seismic events because of its influence on the effective natural period of the structure. In this study, the secant stiffness at different bent top displacements was utilized as the stiffness degradation parameter.

Figure 19B presents the stiffness degradation of the four bent specimens. Among the four specimens, it was found

that the initial stiffness of the DCMB with SCEB-Us is almostly equals to that of the DCMB with link beams and DCMB with EDB-Us. Additionally, the strength degradation of the DCMB with SCEB-Us is minimized, primarily because the strength of the SCEB-Us increases rather than decreases after yielding. The DCMB with link beams exhibited a more significant stiffness degradation due to the severe damage of link beams and columns. The results showed that the application of SCEB-U can effectively enhance the stiffness and minimize stiffness degradation of bents.

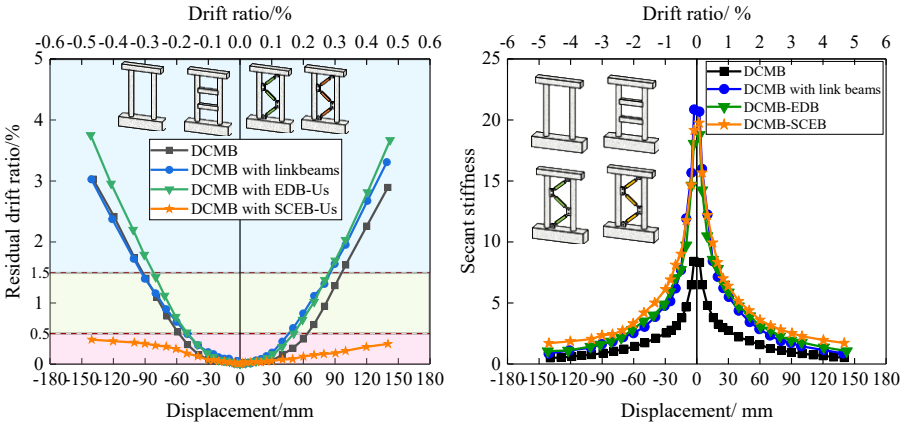

(A) (B)

FIGURE 19 Curves of the four specimens (A) residual drift ratios; (B) stiffness degradation.

6. CONCLUSIONS

The seismic performance of the DCMBs with inverted-K SCEB-Us/EDB-Us were experimentally investigated, and a DCMB with link beams from an actual bridge structure was also considered for comparison. To this end, the simplified analytical model of the DCMB with inverted-K SCEBs was established, and design philosophies of the SCEB in the DCMB were developed. Based on the design philosophies and the hysteretic performance of the DCMB, the U-plate energy dissipation brace as the EDB-Us and self-centering U-plate energy dissipation brace as the SCEB-Us were developed and tested to investigate their hysteretic behavior. Subsequently, the quasi-static cyclic loading test of the 1:4 scaled specimens, including DCMB with link beams, and DCMB with SCEB-Us/EDB-Us, was carried out. The following conclusions can be drawn:

- When the braces are attached in the DCMB in a “K” shaped arrangement scenario, the hysteretic behavior of the DCMB with braces can be regarded as the parallel combination of those of the DCMB and the first layer of brace. The horizontal force components of the two braces acting on the same column-brace joint can cancel each other out when the axial forces of the two braces are equal to each other.
- The SCEB-U exhibits typical flag-shaped hysteresis curves with good energy dissipation ability, excellent self-centering capability, and without obvious stiffness or strength degradation. The EDB-U exhibits plump hysteretic behavior, while the residual deformation is obvious. In particular, both EDB-U and SCEB-U have good deformation ability.
- Compared to the DCMB with link beams, the damage of the DCMB with SCEB-Us/EDB-Us was significantly lighter. The damage regions of the DCMB with SCEB-Us/EDB-Us are mainly focused on the top and bottom of the columns. There was no obvious damage in the regions around the brace-column joints. This is mainly due to the fact that the horizontal force components of the two braces acting on the same column-brace joint can cancel each other out. For the DCMB with link beams, the damage regions were not only concentrated at the top and bottom of the columns, but the link beam- column joint areas also suffered severe damage.
- The DCMB with SCEB-Us exhibits typical flag-shaped hysteresis curves with excellent self-centering capability,

and the SCEB-U and EDB-U as structural fuses yield before the bent. The application of the SCEB-Us to the DCMB obviously increased the strength and stiffness of the bent, and the strength and stiffness of the DCMB with braces approximately equal the sum of those of the DCMB and the first layer of the brace. The DCMB, DCMB with link beams, and DCMB with EDB-Us all represent shuttle-shaped hysteretic behavior with large residual deformation. In addition, no obvious strength degradation occurs for the DCMB with SCEB-Us.

- When the bent is subjected to lateral loads, the deformation curve along the columns presents an inverted triangle, and the deformation increases approximately linearly. When the SCEB-Us were installed in the bent, the residual drift ratios of the bent decreased dramatically to below 0.5% at a lateral drift ratio of 5.0%. Moreover, the external braces can be easily replaced if they are damaged after a severe earthquake.

ACKNOWLEDGMENTS

The authors would like to acknowledge the support from National Natural Science Foundation of China (NSFC) (No. 52278475, 52108430, 52338010), Beijing Municipal Education Commission (No. KM202210005020), and National Key R&D Program of China (No. 2022YFB2602500) for carrying out this research.

CONFLICT OF INTEREST STATEMENT

The authors declare no conflicts of interest.

DATA AVAILABILITY STATEMENT

The data that support the findings of this study are available from the corresponding author upon reasonable request.

ORCID

Huihui Dong https://orcid.org/0000-0001-9174-335X
Xiao Hu https://orcid.org/0009-0007-1197-0044
Kaiming Bi https://orcid.org/0000-0002-5702-6119
Qiang Han https://orcid.org/0000-0003-3973-4119
Alireza Entezami https://orcid.org/0000-0002-4864-2120
Xiuli Du https //orcid.org/0000-0003-2523-3575

REFERENCES:

1. Q. Han, X. Du, J. Liu, Z. Li, L. Li, J. Zhao. Seismic damage of highway bridges during the 2008 Wenchuan earthquake. Earthq. Eng. Eng. Vib. 2009; 8(2) :263-273.
2. J. Li, L. Xu. Seismic responses and damage control of long-span continuous rigid-frame bridges considering the longitudinal pounding effect under strong ground motions. J. Bridge Eng. 2023; 28(2) 04022140.
3. H. Wang, L. Xu, X. Xie, Ge Zhang. Improvement of the seismic resilience of regional buildings: A multi-objective prediction model for earthquake early warning. Soil Dyn. Earthq. Eng. 2024; 179 108545.
4. Z. Lin, L. Xu, X. Xie. Shape function-based multi-objective optimizations of seismic design of buildings with elastoplastic and self-centering components. Comput. Struct. 2024; 296 107303.
5. H. Dong, R. Ma, Q. Han, X. Du. Seismic resilience of RC bridge with self-centering energy dissipation braces using SMA U-shaped plates. Soil Dyn. Earthq. Eng. 2024; 181 108632.
6. S. Hu, R. Zhang, W. Wang. Hybrid self-centering dual rocking core system for seismic resilience by controlling both structural and nonstructural damage. Eng. Struct. 2023; 295 116796.
7. S. El-Bahey, M. Bruneau. Buckling restrained braces as structural fuses for the seismic retrofit of reinforced concrete bridge bents. Eng. Struct. 2011; 33(3): 1052-1061.
8. S. El-Bahey, M. Bruneau. Bridge piers with structural fuses and bi-steel columns. I: Experimental testing, J. Bridge Eng. 2012; 17(1): 25-35.
9. S. El-Bahey, M. Bruneau. Bridge piers with structural fuses and bi-steel columns. II: Analytical investigation, J. Bridge Eng. 2012; 17(1): 36-46.

10. X. Wei, M Bruneau, Case study on applications of structural fuses in bridge bents, J. Bridge Eng.2016; 21(7): 05016004.
11. X. Chen, C. Li. Seismic assessment of tall pier bridges with double-column bents retrofitted with buckling restrained braces subjected to near-fault motions. Eng. Struct. 2021; 226:111390.
12. N. Xiang, M. S. Alam, J. Li. Effect of Multi-Story Brace Distribution on Seismic Performance of RC Tall Bridge Bents Retrofitted with Buckling Restrained Braces. J. Earthqu. Eng. 2022;26(16): 8688-8705.
13. H. Dong, X. Du, Q. Han, K. Bi, H. Hao. Hysteretic performance of RC double-column bridge piers with self-centering buckling-restrained braces. Bull. Earthq. Eng. 2019; 17: 3255-3281.
14. K. R. Mackie, B. Stojadinović. Post-earthquake functionality of highway overpass bridges. Earthq. Eng. Struct. Dyn. 2006; 35(1): 77-93.
15. I. Dangol, C. P. Pantelides. Seismic analysis of posttensioned and hybrid bridge bents with buckling restrained braces. J. Bridge Eng. 2023; 28(2) 04022146.
16. W. Xie, J. Wang, Y. Bao, L. Sun. Theoretical studies and verification on tall RC two-column piers with BRBs: Numerical simulations and shaking table tests, Eng. Struct. 2024; 304 117683.
17. S. Akbari, M. Khanmohammadi. A probabilistic framework to make a decision on the post-earthquake functionality of bridges considering the damage, residual displacement, and aftershock. Bull. Earthq. Eng. 2022; 1-26.
18. X. Wang, A. Shafieezadeh, A. Ye. Optimal EDPs for post-earthquake damage assessment of extended pile-shaft–supported bridges subjected to transverse spreading. Earthq. Spectra 2019; 35(3): 1367-1396.
19. M. R. Eatherton, L. A. Fahnestock, D. J. Miller. Computational study of self-centering buckling-restrained braced frame seismic performance. Earthq. Eng. Struct. Dyn. 2014; 43(13): 1897-1914.
20. W. Wang, C. Fang, Y. Zhao, R. Sause, S. Hu, J. Ricles. Self-centering friction spring dampers for seismic resilience, Earthq. Eng. Struct. Dyn. 2019; 48(9): 1045-1065.
21. F. Shi, Z. Lin, Q. Li, O. E. Ozbulut, Z. He, Y. Zhou. Design, manufacturing, and testing of a hybrid self-centering brace for seismic resilience of buildings. Earthq. Eng. Struct. Dyn.2023; 52(5): 1381-1402.
22. R. Zhang, W. Wang, M. S. Alam. Seismic evaluation of friction spring-based self-centering braced frames based on life-cycle cost. Earthq. Eng. Struct. Dyn. 2022; 51(14): 3393-3415.
23. T. Liu, L. H. Zhu, Y. R. Dong, J. W. Luo, Z. J. Li. Experimental and mathematical model of the variable friction adaptive self-centering energy dissipative brace. Earthq. Eng. Struct. Dyn. 2023; 52(14): 4660-4680.
24. Li J, Wu B, Wang Z, et al. Concept, analysis, and test of a self‐centering viscous damper with displacement capacity enhancement. Earthq. Eng. Struct. Dyn. 2022; 51(11): 2791-2810.
25. Wang H, Nie X, Pan P. Development of a self-centering buckling restrained brace using cross-anchored pre-stressed steel strands. J. Constr. Steel. Res. 2017; 138: 621-632.
26. Kitayama S. Development and evaluation of procedures for analysis and design of buildings with fluidic self-centering systems. State University of New York at Buffalo, 2017.
27. Kitayama S, Constantinou M C. Fluidic self-centering devices as elements of seismically resistant structures: description, testing, modeling, and model validation. J. Struct. Eng. 2017; 143(7): 04017050.
28. Kitayama S, Constantinou M C. Design and analysis of buildings with fluidic self-centering systems. J. Struct. Eng. 2016; 142(11): 04016105.
29. Kitayama S, Constantinou M C. Probabilistic collapse resistance and residual drift assessment of buildings with fluidic self‐centering systems. Earthq. Eng. Struct. Dyn. 2016; 45(12): 1935-1953.
30. Yan X, Alam M S, Rahgozar N, et al. Performance-based seismic design method for disc spring-based self-centering viscous dissipative braced steel frame. J. Build. Eng. 2024; 84: 108493.
31. Shi F, Lin Z, Li Q, et al. Design, manufacturing, and testing of a hybrid self‐centering brace for seismic resilience of buildings. Earthq. Eng. Struct. Dyn. 2023; 52(5): 1381-1402.
32. Eatherton M R, Fahnestock L A, Miller D J. Computational study of self‐centering buckling‐restrained braced frame seismic performance. Earthq. Eng. Struct. Dyn. 2014; 43(13): 1897-1914.
33. C. Christopoulos, A. Filiatrault, B. Folz. Seismic response of self-centering hysteretic SDOF systems. Earthq. Eng. Struct. Dyn. 2002; 31(5): 1131-1150.
34. C. Christopoulos, R. Tremblay, H. J. Kim, M. Lacerte. Self-centering energy dissipative bracing system for the seismic resistance of structures: development and validation. J. Struct. Eng. 2008; 134(1): 96-107.
35. R. Tremblay, M. Lacerte, C. Christopoulos, Seismic response of multistory buildings with self-centering energy dissipative steel braces, J. Struct. Eng. 134(1) (2008) 108-120.
36. L. Xu, X. Fan, Z. Li. Development and experimental verification of a pre-pressed spring self-centering energy

dissipation brace. Eng. Struct. 2016;127: 49-61.
37. L. Xu, X. Fan, Z. Li. Cyclic behavior and failure mechanism of self-centering energy dissipation braces with pre-pressed combination disc springs. Earthq. Eng. Struct. Dyn. 2017; 46(7): 1065-1080.
38. S. Zhu, Y. Zhang. Seismic analysis of concentrically braced frame systems with self-centering friction damping braces. J. Struct. Eng. 2008; 134(1): 121-131
39. N. Xiang, M. S. Alam, Displacement-based seismic design of bridge bents retrofitted with various bracing devices and their seismic fragility assessment under near-fault and far-field ground motions, Soil Dyn. Earthq. Eng. 2019; 119: 75-90.
40. A. Upadhyay, C. P. Pantelides, L. Ibarra. Residual drift mitigation for bridges retrofitted with buckling restrained braces or self centering energy dissipation devices. Eng. Struct. 2019; 199: 109663.
41. H. Dong, X. Du, Q. Han, K. Bi, X. Wang. Performance of an innovative self-centering buckling restrained brace for mitigating seismic responses of bridge structures with double-column piers. Eng. Struct. 2017; 148: 47-62.
42. H. Dong, Y. Bai, Q. Han, X. Du. Mechanical Performance of New type of self-centering energy dissipation brace and its application in double-column bridge structures. Chin J Highw Transp. 30(12):196–204. 2017; 30(12): 196-204. (in Chinese).
43. H. Dong, X. Hu, X. Du, J. Wen, Q. Han. Seismic performance of RC bridges with double-column medium height bents retrofitted with SCEBs under near-field ground motions. Bull. Earthq. Eng. 2024; 1-27.
44. H. Dong, X. Du, Q. Han, K. Bi. Numerical studies on the seismic performances of RC two-column bent bridges with self-centering energy dissipation braces. J. Struct. Eng.2020; 146(4): 04020038.
45. H. Dong, J. Wen, Q. Han, X. Du. Seismic Performance Assessment of a RC Bridge Retrofitted with SCEBs Under Near-Fault Pulse-Like Ground Motions, J. Earthqu. Eng. 2023; 27(13) 3705-3727.
46. MOT (Ministry of Transport). Specifications for seismic design of highway bridges. 2020.
47. Z. Zhang, X. Gao, H. Shen, J. Zhang, L. Wang, H. Qian, P. Sheng. A novel self-centering friction damper with elastic post-buckling plates to retrofit bridge bents, Soil Dyn. Earthq. Eng. 2023; 173 108113.
48. J. Erochko, C. Christopoulos, R. Tremblay, H. Choi. Residual drift response of SMRFs and BRB frames in steel buildings designed according to ASCE 7-05. J Struct Eng 2010;137(5): 589-599.
49. J. A. Oviedo-Amezquita, N. Jaramillo-Santana, C. A Blandon-Uribe, A. M. Bernal-Zuluaga. Development and validation of an acceptance criteria and damage index for buckling-restrained braces (BRB). J. Build. Eng. 2021; 43 102534.
50. GB T1972-2005. 2005. Disc spring. Beijing: China Architecture Industry Press.
51. AASHTO (2009) Guide specifications for LRFD seismic bridge design. American Association of State Highway and Transportation Offcials, Washington, DC.
52. R. Park. State-of-the-art report ductility evaluation from laboratory and analytical testing. Proceedings of 9th World Conference on Earthquake Engineering. Tokyo, Kyoto, Japan 1988; 605-616.
53. R. Bazaez, P. Dusicka. Cyclic behavior of reinforced concrete bridge bent retrofitted with buckling restrained braces. Eng. Struct. 2016;119: 34-48.